Hindawi
International Journal of Aerospace Engineering
Volume 2023, Article ID 6659124, 12 pages
https://doi.org/10.1155/2023/6659124

Research Article

Modular Dynamic Modeling for On-Orbit Assembly of Large-Scale Space Structures

Weiya Zhou,[1] **Shunan Wu**,[2] **and Jinzhao Yang**[2]

[1]*School of Aeronautics and Astronautics, Dalian University of Technology, Dalian 116024, China*
[2]*School of Aeronautics and Astronautics, Sun Yat-sen University, Shenzhen 518107, China*

Correspondence should be addressed to Shunan Wu; wushunan@mail.sysu.edu.cn

Received 4 August 2023; Revised 25 September 2023; Accepted 26 September 2023; Published 7 October 2023

Academic Editor: Chuang Liu

The large-scale space structure during on-orbit assembly is a time-varying system. The dynamic modeling problem of such incrementally increasing space structure is investigated, and a modular dynamic modeling approach is proposed in this paper. The dynamic model of each substructure is first established, and then, a database is designed to store substructure models, which is used for subsequent dynamic modeling in the assembly process. The fixed connection relationship between adjacent substructures is described by constraint conditions, which lead to the coefficient matrices of adjacent substructures being decoupled. The substructures are assembled in a given sequence, and then, the dynamic modeling, to describe the large-scale space structure on-orbit assembly, is gradually completed via using the proposed modeling approach. The numerical simulation is finally presented. The results demonstrate that the extra calculation resulting from the coefficient matrices coupling of adjacent substructures is avoided. Moreover, the proposed dynamic model can accurately describe the dynamic characteristics of the large-scale space structure during on-orbit assembly.

1. Introduction

With the increasing demand of space missions, spacecraft is developing towards the trend of large-scale and lightweight, such as large space telescopes [1], communication antennas [2], and solar power satellite [3]. However, the large-scale space structure (LSS) cannot be constructed in one deployment, due to the constraints of a payload fairing of a rocket. To solve this problem, the LSS is designed as multiple modular substructures, which are sent into space by multiple launches, and then, they are assembled on orbit by robots [1, 4]. The number of modular substructures significantly increases along with on-orbit assembly. The configuration also gradually grows, and dynamic parameters of the LSS then jumpingly change, and the dynamic characteristics of the whole system become very complicated during on-orbit assembly, which brings a new challenge to the dynamic modeling and structural active control.

Hence, it is very important to develop a dynamic model of the LSS during on-orbit assembly, which could be accurately used to describe the dynamic characteristics of the incrementally increasing space structure. Recently, many scholars have carried out extensive research on the on-orbit assembly of LSSs. The coupled vibration problem between robots and LSS is studied during the handing process [5]. The coupling dynamic model between a two-legged mobile robot and a LSS is developed during in-space structure assembly [6]. The dynamic model of the robot base and the flexible structure is established, and the assembly experiments of flexible structures are presented [7]. The above work mainly focuses on the coupled modeling between the space robot and assembly structures. The disturbance rejection in the space environment is also a very important research area [8, 9]. The influence of disturbances on dynamic modeling and analysis, such as contact-impact or orbit transfer, is to get more attention, rather than the changes of the LSS itself. The LSS is constructed via on-orbit assembly in a given sequence. The number of substructures gradually increases, and the flexible characteristics of the LSS become more obvious as the assembly proceeds. For instance, the solar power satellite contains multiple flexible appendages, the structure size is huge, and a higher

dimensional model is usually needed to ensure accuracy [10]. However, the structure dynamic modeling in the assembly stage is significantly different from that of the on-orbit operation stage, and its dynamic modeling and analysis are also very important [11]. Besides, the existing modeling methods mainly focus on the LSS after assembly. Most of dynamic models are derived for the invariant space structures, namely, the geometry and parameters do not change [12]. The gradually increasing condition in the assembly process has been not considered. Thus, it is difficult to describe the dynamic characteristics of LSSs and achieve a good vibration suppression effect during assembly using the previous models. There are also some interesting and worthwhile works about on-orbit assembly. A dynamic modeling method for active control of on-orbit assembly with "node freedom degree loading" is proposed [13]. The problem of sequential assembly and shape control of the reflector antenna are studied, which is based on the life and death element technology in the finite element method [14]. An on-orbit assembly strategy for an orb-shaped solar array is developed, and the dynamic model for the structural vibration under the influence of the gradient is also presented [15]. Despite many valuable contributions in previous literature, it should be emphasized that the criteria for variation of the LSS dynamic modeling in the assembly process have not been clearly investigated. These assembly modeling methods for the incremental structures have low applicability, and some methods can not even guarantee the accuracy of the dynamic modeling. Besides, it usually required repeated superposition calculation of the coefficient matrices in the assembly process, which is tedious and complex. To sum up, the dynamic modeling problem for on-orbit assembly of the LSS is investigated. The main contributions are summarized as follows: (1) A modular dynamic modeling approach (MDMA) of LSSs during on-orbit assembly is proposed. The dynamic models of each substructure are first established, and the fixed connection relationship between adjacent substructures is then described by constraint conditions, during the assembly process. Then, the proposed dynamic model can accurately describe the dynamic characteristics of the incrementally increasing space structure. (2) The coefficient matrices of the adjacent substructure are decoupled, and the reconfiguration of the existing coefficient matrices is not required along with the assembly using the proposed dynamic model, which is formulated as a set of differential-algebraic equations. Compared with [16, 17], the extra calculation due to the coupling of state coefficient matrices of the LSS at each assembly stage is avoided. Moreover, the dynamic parameters of the substructure only need to be calculated separately, which is convenient for the design of the distributed control system with good expansibility.

The paper is organized as follows. The preparation of the dynamic modeling is presented in Section 2, which contains developing each substructure dynamic model and presenting modeling assumptions. The distributed cooperative control approach for vibration suppression in the assembly process is presented in Section 3. Section 4 presents simulation results to demonstrate the accuracy of the proposed model and to achieve vibration suppression of the LSS during on-orbit assembly. The conclusion is introduced in Section 5.

2. Preparation of Dynamic Modeling

2.1. Dynamic Modeling Process of LSS On-Orbit Assembly. The LSS is composed of multiple modular substructures, and the construction is completed via on-orbit assembly. The types of assembly substructures are different. It can be distinguished by geometric configuration, material parameters, etc. The assembly process of substructures is generally regular and repetitive. Thus, a model database of the assembled substructures is developed to store the dynamic models, constraint conditions, and geometric material parameters of substructures. The dynamic parameters of the assembled substructures in the model database can be used directly during the dynamic modeling. It avoids the remodeling of the substructure in the assembly process. In the process of LSS assembly, the dynamic model of the substructure is first obtained from the database, and the connection of adjacent substructures is defined by geometric constraint. When one more substructure is assembled, only a submatrix needs to be placed at the corresponding position in the coefficient matrices of the whole structure, and the coefficient matrices of the previous substructure do not change. The update process of the coefficient matrices is shown in Figure 1.

To better illustrate the MDMA, the procedure to perform the approach is designed as shown in Figure 2, and the detailed process consists of the following steps:

(1) Considering the task requirements, large size, and complex configuration, the LSS is designed into N modular substructures, and the assembly process is divided into N stage

(2) The dynamic model of each substructure is derived, and then, the substructure database is developed to store the models of these substructures

(3) The constraint conditions of the assembled substructure are derived according to the assembly position, the number of interfaces, and geometric configuration, and then, these parameters are stored in the database

(4) The dynamic parameters of the substructure, which will be assembled immediately, are obtained from the database, and the substructure is then gradually assembled via a given sequence. The dynamic model of the LSS at each assembly stage is then updated, and the dynamic characteristic analysis and vibration control are also realized in assembly process

(5) Repeat the above steps until all substructures are assembled, and the dynamic model of the whole LSS after finishing assembly is therefore obtained

2.2. Constraint Equations. Some LSSs are consisted of multiple modules. For example, the solar power satellite contains truss module, solar array module, and antenna module. These modules can be divided into N substructures and

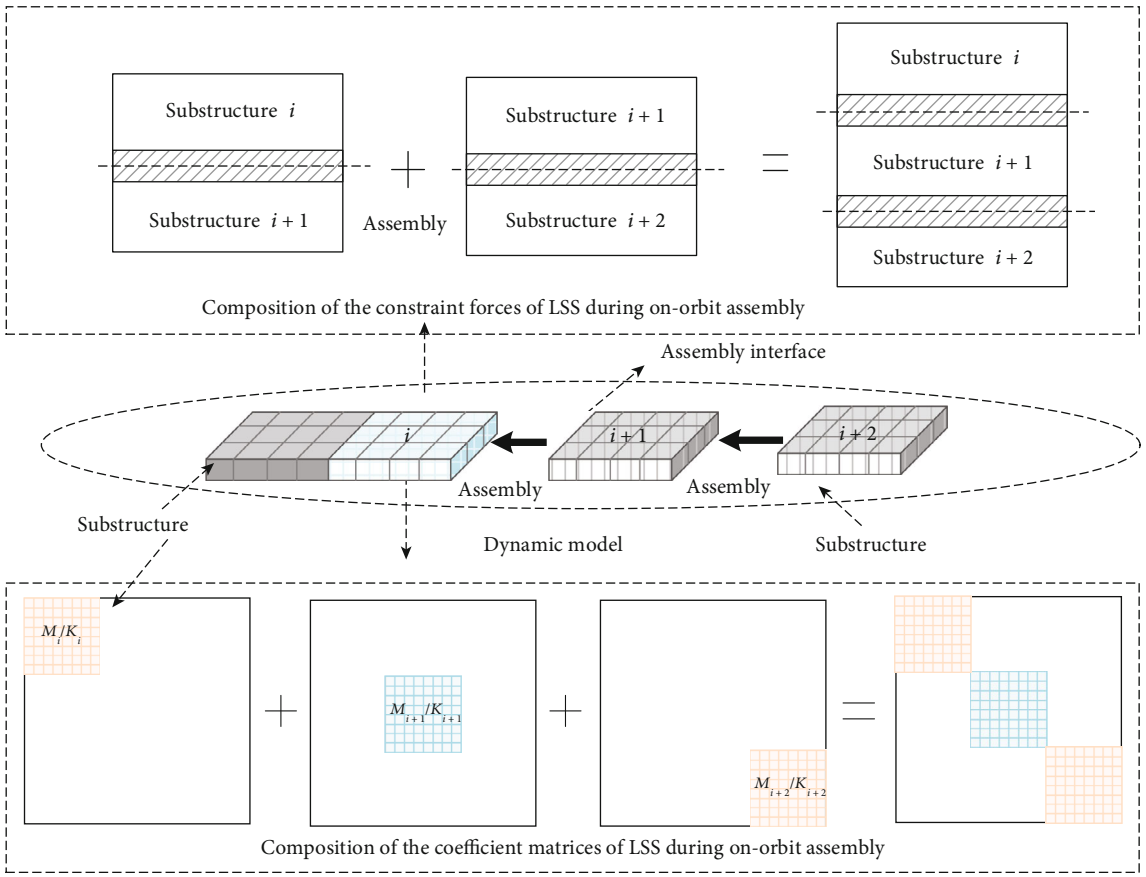

Figure 1: The update process of the dynamic parameters during on-orbit assembly.

are assembled on orbit [18]. The plate structure and truss structure are then used for the equivalent dynamic modeling. However, the dynamic models are derived for the plate elements, and rod elements are different, and thus, the constraint equation of solar array substructure and truss substructure is also different.

2.2.1. Geometric Constraints. There are geometric constraints between adjacent assembly substructures due to the fixed connections. The substructure i is adjacent to substructure $i+1$, and the jth node on the substructure i corresponds to the kth node on the substructure $i+1$, as shown in Figure 3.

For the dynamic modeling of solar array module assembly, four-node rectangular plate elements are used to derive the dynamic model. Multiple solar array substructures are assembled on orbit, and then, the construction of the solar array of the solar power satellite is completed. The substructures of each solar array are fixedly connected after assembly. Thus, the following constraints between the adjacent substructures are

$$\tilde{\psi}_{i,j} = \begin{bmatrix} \rho_{i,j} + l_c\theta_{i,j} - \rho_{i+1,k} \\ \theta_{i,j} - \theta_{i+1,k} \end{bmatrix} = 0, \quad (1)$$

where θ is the rotation angle of the substructure, l_c represents the distance between two adjacent substructures, and ρ denotes the deflection.

For the dynamic modeling of truss structure assembly, the rod element is adopted. Thus, the geometric constraint equation of truss substructures is given by

$$\tilde{\psi}_{i,j} = r_{i,j} - r_{i+1,k} = 0, \quad (2)$$

where r is the node position vector.

The geometric constraint equation of adjacent substructures in the whole LSS can be written as follows.

$$\tilde{\psi}_1 = \left[\tilde{\psi}_{1,1}^T \quad \tilde{\psi}_{1,2}^T \quad \cdots \quad \tilde{\psi}_{1,m}^T \cdots \tilde{\psi}_{i,j}^T \cdots \tilde{\psi}_{n,m}^T\right]^T, \quad (3)$$

where n denotes the number of substructures and m is the number of nodes in the connecting edges of adjacent substructures.

2.2.2. Boundary Conditions. The second part is the induction of boundary conditions. The left end of LSS is the fixed end. Therefore, for the left end of solar array structure, the constraint equations are as follows:

$$\tilde{\psi}_2 = \begin{bmatrix} \rho_0 \\ \theta_0 \end{bmatrix} = 0, \quad (4)$$

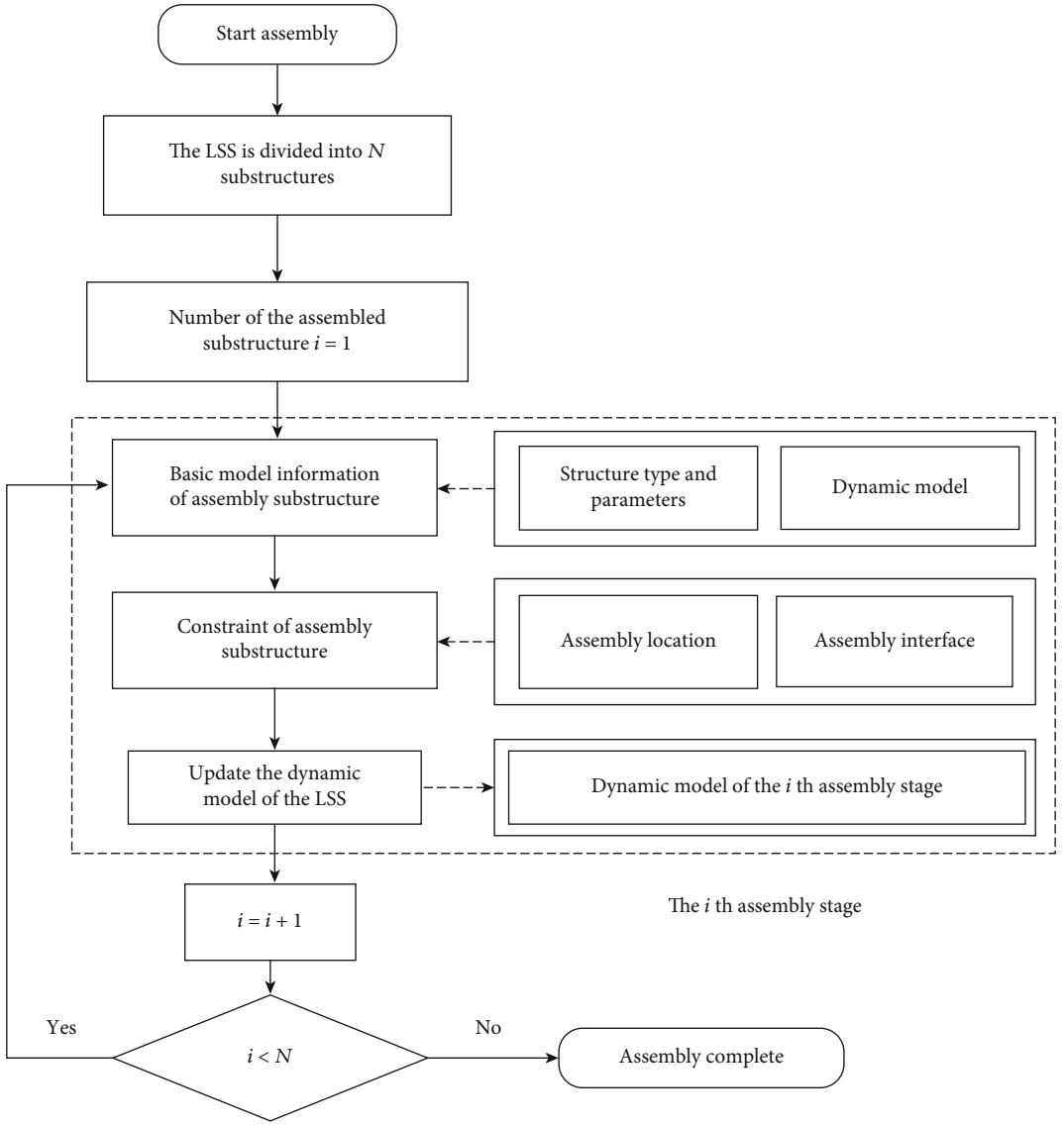

Figure 2: Modeling process for LSS on-orbit assembly.

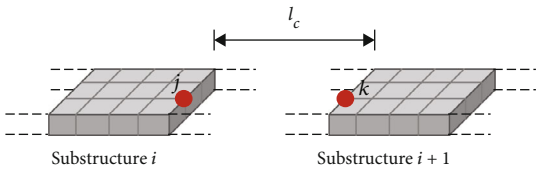

Figure 3: Schematic diagram of the substructure geometric constraint.

where ρ_0 and θ_0 denote the deflection and rotation angles on the first substructure.

For the dynamic modeling of truss structure assembly, the boundary conditions for the left end of the truss substructure are described by

$$\tilde{\psi}_2 = r_0 = 0, \tag{5}$$

where r_0 is the node position vector on the first substructure.

All the constraint equations are given by

$$\psi = \begin{bmatrix} \tilde{\psi}_1^T & \tilde{\psi}_2^T \end{bmatrix}^T = 0 \tag{6}$$

3. Dynamic Model in Assembly Process

The actuation force on LSS during on-orbit assembly, including assembly impact disturbance forces and control forces, is described as

$$F_i = b_i u_i + d_i w_i, \tag{7}$$

where i is the ith assembly substructure, b_i is the control input matrix, d_i is the disturbance matrix, u_i denotes the control input, and $\bar{w}_i$ is the disturbance force.

The stiffness matrix, mass matrix, and damping matrix of the substructure to be assembled are obtained via substructure database. Then, the constraint conditions are used

to describe the connection relationship between the adjacent assembly substructure. According to the Lagrange equation, the dynamic model of LSS in the first assembly stage is developed. It is formulated as a set of differential-algebraic equations as follows:

$$\begin{aligned} \boldsymbol{M}_1\ddot{\boldsymbol{q}}_1 + \boldsymbol{C}_1\dot{\boldsymbol{q}}_1 + \boldsymbol{K}_1\boldsymbol{q}_1 + \left(\frac{\partial \boldsymbol{\psi}_1}{\partial \boldsymbol{q}_1}\right)^T \boldsymbol{\lambda}_1 &= \boldsymbol{F}_1, \\ \boldsymbol{\psi}_1 &= 0, \end{aligned} \tag{8}$$

where M_1, C_1, and K_1 are the mass matrix, damping matrix, and stiffness matrix of the LSS after the first assembly, respectively; q_1, λ_1, ψ_1 and F_1 are the generalized coordinates, Lagrange multiplier, constraint condition, and generalized forces of the LSS after the first assembly.

During the $i+1$th assembly stage, the constraint conditions and dynamic model of the $i+1$ th substructure are first obtained from the substructure database. The update process of coefficient matrices of the LSS during on-orbit assembly is shown in Figure 1. The coefficient matrices of the dynamic equation assembled previously do not change. The connection between the assembly substructure and LSS is then established by geometric constraint Eq. (1) or Eq. (2). The dynamic model of LSS in the $i+1$th assembly stage is given by

$$\begin{aligned} \boldsymbol{M}_{i+1}\ddot{\boldsymbol{q}}_{i+1} + \boldsymbol{C}_{i+1}\dot{\boldsymbol{q}}_{i+1} + \boldsymbol{K}_{i+1}\boldsymbol{q}_{i+1} + \left(\frac{\partial \boldsymbol{\psi}_{i+1}}{\partial \boldsymbol{q}_{i+1}}\right)^T \boldsymbol{\lambda}_{i+1} &= \boldsymbol{F}_{i+1}, \\ \boldsymbol{\psi}_{i+1} &= \boldsymbol{0}, \end{aligned} \tag{9}$$

where M_{i+1}, C_{i+1}, and K_{i+1} denote the mass matrix, damping matrix, and stiffness matrix of the LSS after the $i+1$th assembly; F_{i+1}, q_{i+1}, λ_{i+1}, and ψ_{i+1} are the generalized forces, generalized coordinates, Lagrange multiplier vector, and constraint conditions of the LSS after the $i+1$th assembly. M_{i+1}, C_{i+1}, and K_{i+1} are

$$\begin{aligned} M_{i+1} &= \begin{bmatrix} M_i & 0 \\ 0 & \bar{M}_{i+1} \end{bmatrix}, \\ C_{i+1} &= \begin{bmatrix} C_i & 0 \\ 0 & \bar{C}_{i+1} \end{bmatrix}, \\ K_{i+1} &= \begin{bmatrix} K_i & 0 \\ 0 & \bar{K}_{i+1} \end{bmatrix}, \end{aligned} \tag{10}$$

where M_i, C_i, and K_i are the mass matrix, damping matrix, and stiffness matrix of the LSS after the ith assembly; $\bar{M}_{i+1}$, $\bar{C}_{i+1}$, and $\bar{K}_{i+1}$ denote the mass matrix, damping matrix, and stiffness matrix of the $i+1$th assembly substructure.

$$\begin{aligned} F_{i+1} &= \begin{bmatrix} F_i \\ \bar{F}_{i+1} \end{bmatrix}, \\ q_{i+1} &= \begin{bmatrix} q_i \\ \bar{q}_{i+1} \end{bmatrix}, \\ \lambda_{i+1} &= \begin{bmatrix} \lambda_i \\ \bar{\lambda}_{i+1} \end{bmatrix}, \\ \psi_{i+1} &= \begin{bmatrix} \psi_i^T & \bar{\psi}_{i+1}^T \end{bmatrix}^T, \\ \left(\frac{\partial \psi_{i+1}}{\partial q_{i+1}}\right)^T &= \begin{bmatrix} \dfrac{\partial \psi_i}{\partial q_i} & 0 \\ \dfrac{\partial \bar{\psi}_{i+1}}{\partial q_i} & \dfrac{\partial \bar{\psi}_{i+1}}{\partial \bar{q}_{i+1}} \end{bmatrix}^T, \end{aligned} \tag{11}$$

where F_i, q_i, λ_i, and ψ_i represent the generalized forces, generalized coordinates, Lagrange multiplier vector, and constraint conditions of the LSS after the ith assembly; $\bar{F}_{i+1}$, $\bar{q}_{i+1}$, $\bar{\lambda}_{i+1}$, and $\bar{\psi}_{i+1}$ are the generalized forces, generalized coordinates, Lagrange multiplier vector, and constraint conditions of the $i+1$th assembly substructure.

The LSS is gradually assembled according to the process, as shown in Figure 2. After the assembly is completed, the dynamic model of the whole LSS is given by

$$\begin{aligned} \boldsymbol{M}\ddot{\boldsymbol{q}} + \boldsymbol{C}\dot{\boldsymbol{q}} + \boldsymbol{K}\boldsymbol{q} + \left(\frac{\partial \boldsymbol{\psi}}{\partial \boldsymbol{q}}\right)^T \boldsymbol{\lambda} &= \boldsymbol{F}, \\ \boldsymbol{\psi} &= \boldsymbol{0}, \end{aligned} \tag{12}$$

where M, C, and K are the mass matrix, damping matrix, and stiffness matrix of the whole LSS after assembly completed; F, λ, ψ, and q denote the generalized forces, Lagrange multiplier vector, constraint conditions, and generalized coordinates of the whole LSS after assembly completed. Namely

$$M = \begin{bmatrix} \bar{M}_1 & \cdots & 0 & \cdots & 0 \\ \vdots & \ddots & \vdots & \vdots & \vdots \\ 0 & \cdots & \bar{M}_i & \cdots & 0 \\ \vdots & \vdots & \vdots & \ddots & \vdots \\ 0 & \cdots & 0 & \cdots & \bar{M}_n \end{bmatrix},$$

$$C = \begin{bmatrix} \bar{C}_1 & \cdots & 0 & \cdots & 0 \\ \vdots & \ddots & \vdots & \vdots & \vdots \\ 0 & \cdots & \bar{C}_i & \cdots & 0 \\ \vdots & \vdots & \vdots & \ddots & \vdots \\ 0 & \cdots & 0 & \cdots & \bar{C}_n \end{bmatrix},$$

$$K = \begin{bmatrix} \bar{K}_1 & \cdots & 0 & \cdots & 0 \\ \vdots & \ddots & \vdots & \vdots & \vdots \\ 0 & \cdots & \bar{K}_i & \cdots & 0 \\ \vdots & \vdots & \vdots & \ddots & \vdots \\ 0 & \cdots & 0 & \cdots & \bar{K}_n \end{bmatrix}. \tag{13}$$

Equation (12) is a constrained differential-algebraic equation. When solving by difference discretization, the approximation of the higher frequency modes of the system is poor due to the influence of discretization, and hence, the system generates spurious high-frequency response components. If the numerical integration method does not effectively filter out the spurious higher-frequency response components, the accuracy of the numerical solution is reduced. The generalized α method can adjust the spectral radius to tune the algorithmic damping, which then helps to achieve spurious high-frequency dissipation while maintaining the low-frequency response of the system [19]. Hence, the generalized α method is used to solve the dynamic equation of the system in this paper.

To facilitate the solution of the system equation and the design of the control system, for the system equations of the LSS, the state variables of the continuous controlled system are first introduced.

$$x = \begin{bmatrix} q^T & \lambda^T \end{bmatrix}^T. \tag{14}$$

The system states that x of the LSS is the subject to the following equations:

$$G(x, \dot{x}, \ddot{x}) = f(x, \dot{x}, \ddot{x}) \text{-} BU - DW, \tag{15}$$

$$f(x, \dot{x}, \ddot{x}) = \begin{bmatrix} M\ddot{q} + C\dot{q} + Kq + \left(\dfrac{\partial \psi}{\partial q}\right)^T \lambda \\ \psi \end{bmatrix}, \tag{16}$$

Table 1: Geometric and material parameters of the truss substructure.

Parameters	Value
Length (m)	19.5
Damping coefficient	0.002
Young's modulus (Gpa)	70
Poisson's ratio	0.27
Density (kg/m^3)	2700
Cross-sectional area of truss rod (m^2)	$1e-4$
The length of truss rod 1 (m)	1.5
The length of truss rod 2 (m)	2.12

$$\begin{aligned} B &= \begin{bmatrix} b & 0 \\ 0 & 0 \end{bmatrix}, \\ D &= \begin{bmatrix} d & 0 \\ 0 & 0 \end{bmatrix}, \end{aligned} \tag{17}$$

where U and W are the control input and the disturbance force.

At time t_k and t_{k+1}, the system states of the LSS are written as

$$\begin{aligned} x(t_k) &= \begin{bmatrix} q^T(t_k) & \lambda^T(t_k) \end{bmatrix}^T, \\ x(t_{k+1}) &= \begin{bmatrix} q^T(t_{k+1}) & \lambda^T(t_{k+1}) \end{bmatrix}^T. \end{aligned} \tag{18}$$

Then, Eq. (15) is transformed into the following forms:

$$\begin{aligned} G(x(t_{k+1}), \dot{x}(t_{k+1}), \ddot{x}(t_{k+1})) = f(x(t_{k+1}), \dot{\boldsymbol{x}}(t_{k+1}), \ddot{\boldsymbol{x}}(t_{k+1})) \\ - \mathrm{BU}(t_{k+1}) - \mathrm{DW}(t_{k+1}), \end{aligned} \tag{19}$$

Combing the discretization scheme of the generalized-α method and the Newton-Raphson iteration of Eq. (19), $x(t_{k+1})$ is given by

$$x^{(j+1)}(t_{k+1}) = \zeta_1^{(j)}(t_{k+1}) + \zeta_2^{(j)}(t_{k+1})U(t_{k+1}) + \zeta_3^{(j)}(t_{k+1})W(t_{k+1}), \tag{20}$$

$$\begin{aligned} \zeta_1^{(j)}(t_{k+1}) &= x^{(j)}(t_{k+1}) - \left[\left(G^{(j)}(x(t_{k+1}), \dot{x}(t_{k+1}), \ddot{x}(t_{k+1}))\right)'\right]^{-1} f^{(j)}(x(t_{k+1}), \dot{x}(t_{k+1}), \ddot{x}(t_{k+1})), \\ \zeta_2^{(j)}(t_{k+1}) &= \left[\left(G^{(j)}(x(t_{k+1}), \dot{x}(t_{k+1}), \ddot{x}(t_{k+1}))\right)'\right]^{-1} B^{(j)}(t_{k+1}), \\ \zeta_3^{(j)}(t_{k+1}) &= \left[\left(G^{(j)}(x(t_{k+1}), \dot{x}(t_{k+1}), \ddot{x}(t_{k+1}))\right)'\right]^{-1} D^{(j)}(t_{k+1}), \end{aligned} \tag{21}$$

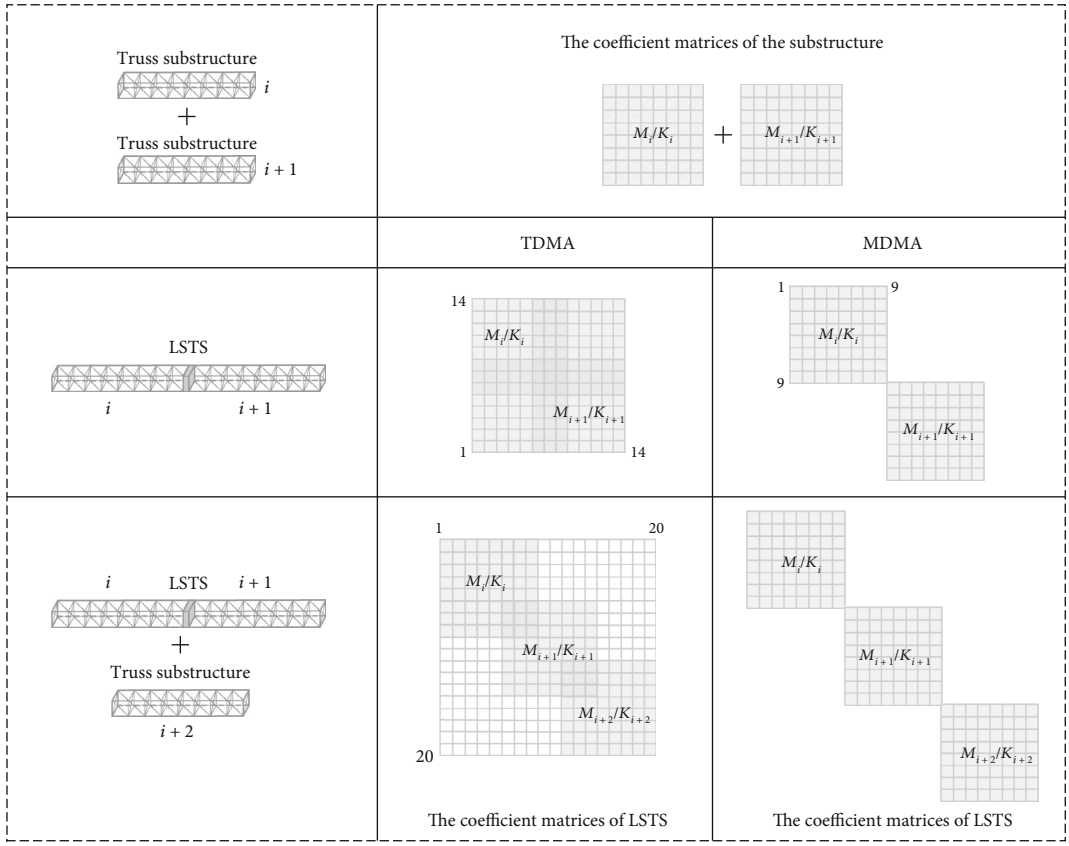

Figure 4: Updating of the coefficient matrices of LSTS during on-orbit assembly.

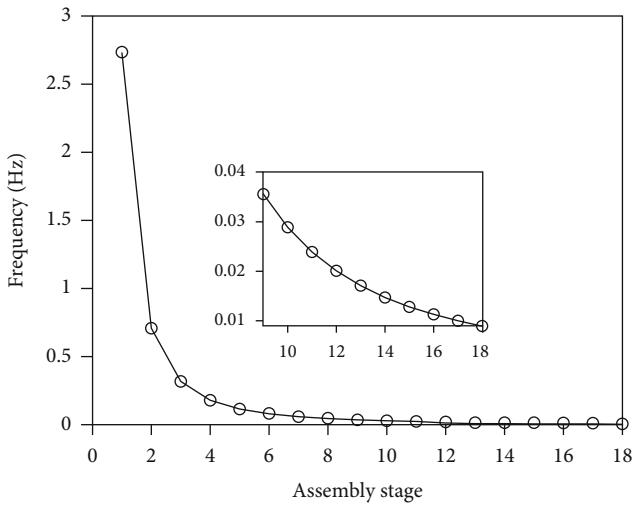

Figure 5: Structural frequency of the LSTS of each assembly stage.

where the superscript j denotes the variables at the jth Newton-Raphson iteration, the symbol $x^{(j+1)}(t_{k+1})$ is the variable vector of the current $j+1$th iteration at time t_{k+1}, and $x^{(j)}(t_{k+1})$ is the variable vector from the previous jth iteration, which is taken as the reference for the current computation.

So far, the iteration variables $x^{(j+1)}(t_{k+1})$ of Eq. (20) are derived and expressed by the control input $U(t_{k+1})$.

Therefore, the system output y of the ith substructure is presented as

$$y(t_{k+1}) = C_y x^{(j+1)}(t_{k+1}), \tag{22}$$

where C_y is the output matrix of the ith substructure and $x(t_{k+1})$ is derived from Eq. (20).

4. Numerical Simulation

4.1. Validation of Dynamic Model. The large space truss structure (LSTS) is the basic component of solar power satellites, which plays an important role in supporting, extending, and fixing large facilities. Hence, the numerical simulations of the LSTS during on-orbit assembly are presented, compared with the finite element method, which is a traditional dynamic modeling approach (TDMA). It can discretize the structure, and the dynamic equation of the structure is then established. Each truss substructure has the same geometric and material parameter configuration. The detailed parameters are presented in Table 1.

In the modeling process of LSTS assembly, the dynamic models established by TDMA usually consist of a set of ordinary differential equations. The coefficient matrices of adjacent substructures are coupled, and it is necessary to calculate several times along with assembly. However, the proposed dynamic model is formulated as a set of differential-

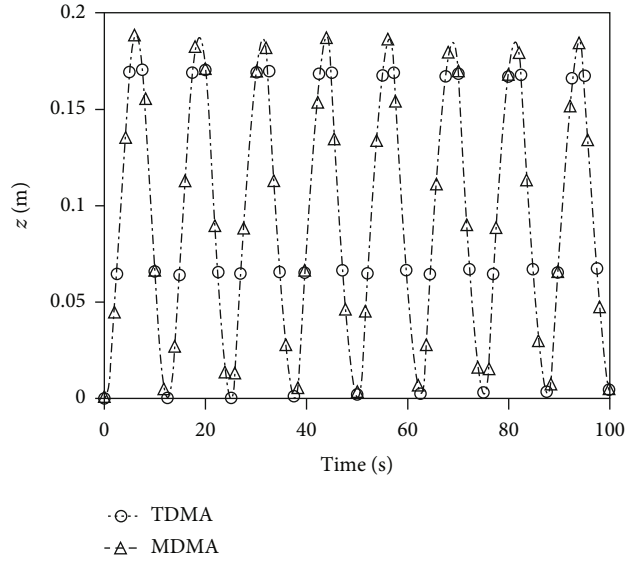

(a) The 6th assembly stage

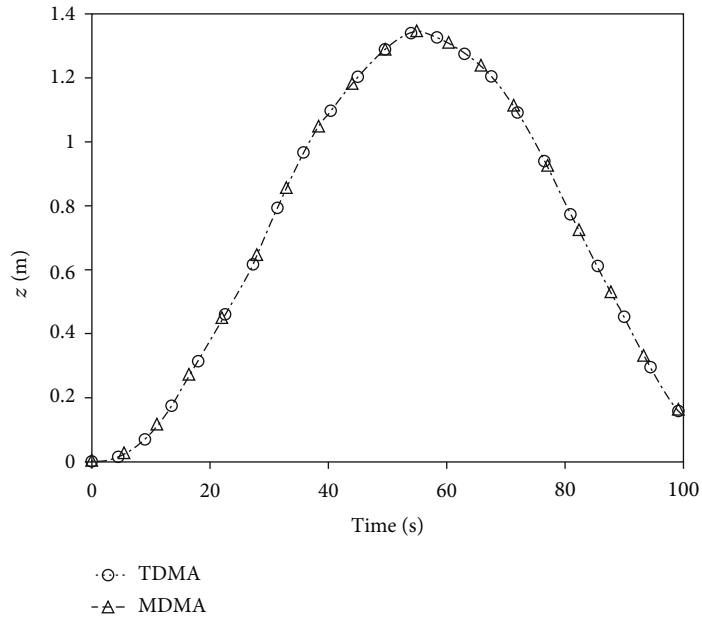

(b) The 18th assembly stage

Figure 6: The displacement curves of LSTS.

algebraic equations, resulting in the coefficient matrices of adjacent assembly substructure being decoupled, as shown in Figure 4. This approach does not require reformulation of the existing coefficient matrices as the number of substructures increases. Thus, it avoids the extra calculation due to the existence of common nodes in adjacent substructures, when the configuration of LSTS changes at each assembly stage.

The length of one side of the LSTS is approximately 351 m, and the length of each truss substructure is 19.5 m. Thus, the whole assembly process is divided into 18 stages. The LSTS is rigid locked after assembly, and the connecting among the adjacent truss substructures is not considered. The dynamic characteristics of LSTS are gradually changing along with the assembly. The natural frequencies of LSTS are analyzed as an example. The process of variation of the first natural frequency of the LSTS after each assembly is presented in Figure 5. As can be seen, the first natural frequency decreases obviously along with assembly.

The simulation results of the LSTS during on-orbit assembly, which is based on the proposed MDMA, are presented in this section. The length of the LSTS is 117 m after the 6th group truss substructure is assembled. The driving forces of each substructure end node are 0.5 N, and the z -axis displacement at the end nodes of the LSTS is obtained. The response curves of the 6 substructures are given in Figure 6(a). The length of the LSTS is 351 m after the 18th group truss substructure is assembled. The driving forces of each substructure end node are 0.05 N, and the z-axis

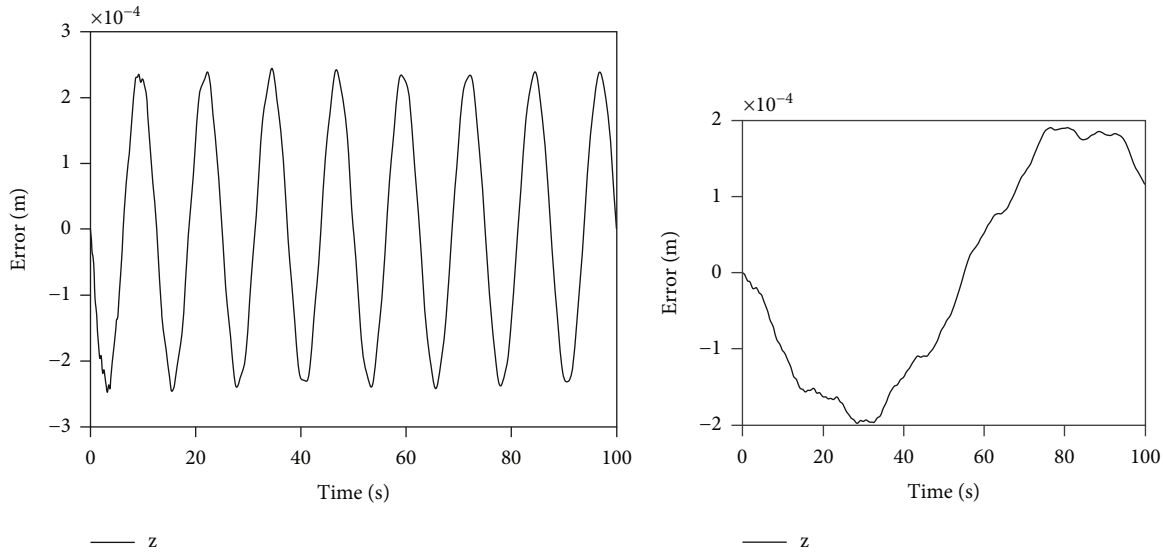

(a) The 6th assembly stage (b) The 18th assembly stage

Figure 7: The error curves of LSTS.

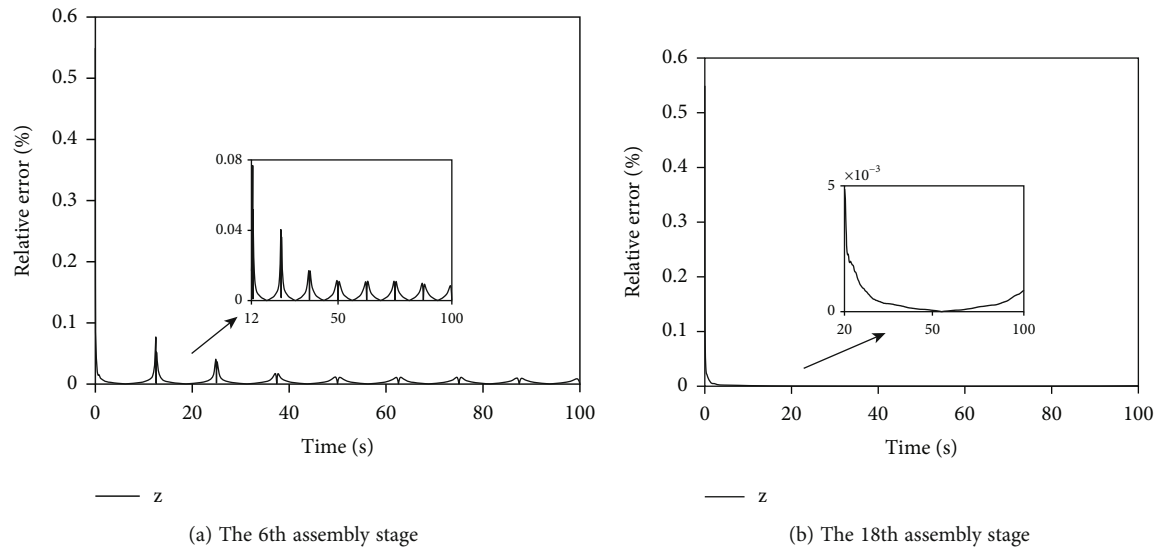

(a) The 6th assembly stage (b) The 18th assembly stage

Figure 8: The relative error curves of LSTS.

displacement at the end nodes is obtained. The response curves of the 18 substructures are given in Figure 6(b).

For the assembly of the 6th substructures, the maximum error is 2.471×10^{-4} m at 3.23 seconds; for the assembly of the 18th substructures, the maximum error is 1.982×10^{-4} m at 28.4th seconds, as shown in Figure 7. However, the maximum relative errors of the assembled LSTS are 0.549% at the initial time. This is due to the vibration amplitude at the initial time being very small, close to 0. Besides, for the LSTS containing 6 substructures, the relative error is fluctuated due to the value of the trough that is close to 0 in the simulation process. The relative error of 6 substructures and 18 substructures was kept around 0.07% and 0.005%, respectively, and gradually decreased, as shown in Figure 8. The numerical simulation results illustrate that the proposed MDMA has the same accuracy as the TDMA.

4.2. Distributed Vibration Control in the Assembly Process. To further verify the validity of the proposed MDMA in this paper and achieve the vibration control during on-orbit assembly, the controller is designed for each assembly substructure, as shown in Figure 9. The sensors and actuators are placed in colocated configuration in the middle of the substructure of each group truss structures.

Due to the rigid connection between substructures after assembly, each controller output applied to one substructure may increase the vibration of the adjacent substructure. The disturbance can be reduced by adding coordination terms to

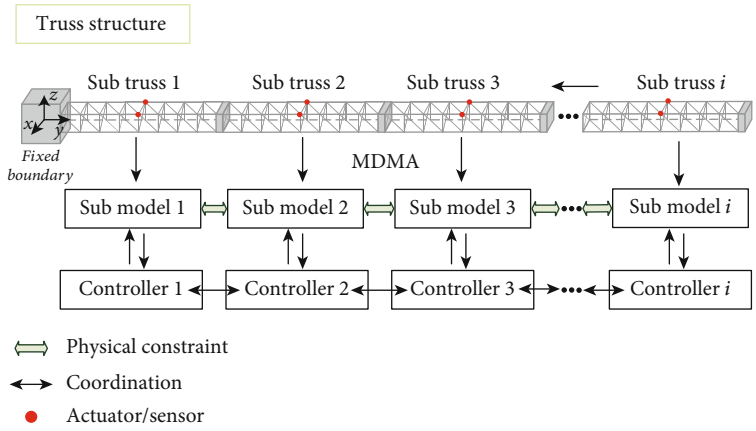

Figure 9: The diagram of the distributed active control strategy in the assembly process.

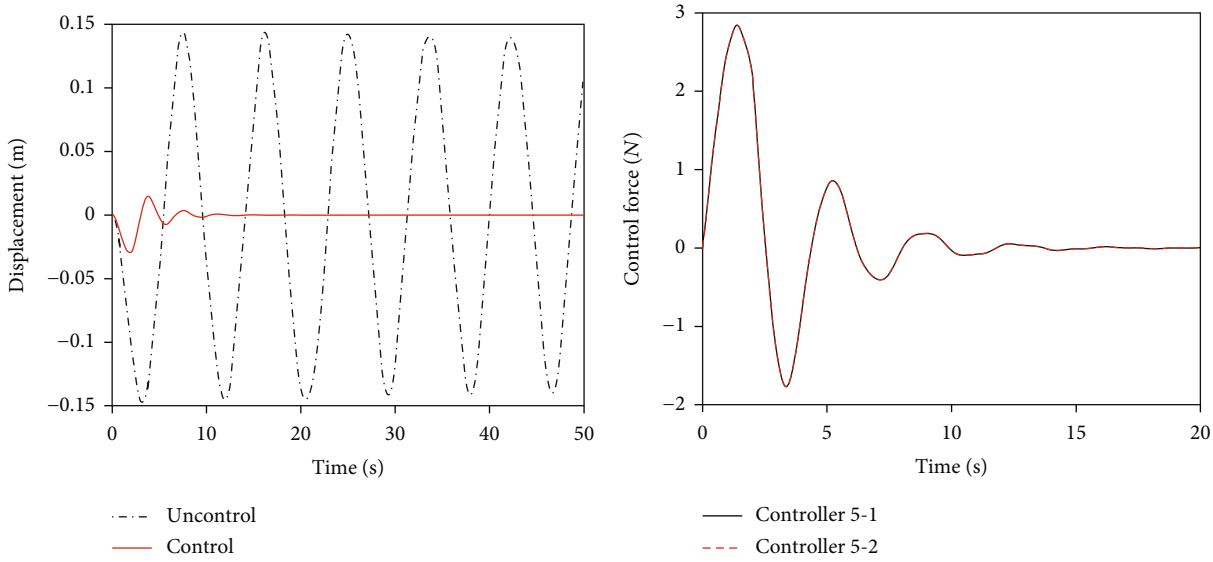

(a) The end dynamic response of truss structure

(b) The control force of the 5th substructure

Figure 10: The dynamic response and the control force during the 5th assembly stage.

the assembly substructure controller. The coordination term is designed based on the measurement information of the adjacent substructures. Then, the distributed control system in the assembly process is gradually formed according to the cooperation of the substructure controller. Therefore, a distributed cooperative controller is used for vibration suppression of the LSTS during on-orbit assembly. The controller consists of two parts: a feedback stabilization term and a consensus coordination term [20]. The controller of the ith assembly substructure is given by

$$U_i(t_{k+1}) = \underbrace{K_{pi}y_i(t_{k+1}) + K_{di}\dot{y}_i(t_{k+1})}_{\text{Feedback stabilization term}} + \underbrace{\sum_{j=1}^{g_i}\left(K_{pj}\left(y_i(t_{k+1}) - y_{ij}(t_{k+1})\right) + K_{dj}\left(\dot{y}_i(t_{k+1}) - \dot{y}_{ij}(t_{k+1})\right)\right)}_{\text{Consensus coordination term}}, \tag{23}$$

where the subscript i denotes the ith substructure and the subscript j is the jth substructure, which is adjacent to the ith substructure; g_i is the number of substructures adjacent to the ith substructure; K_{pi} and K_{di} are the feedback stabilization term coefficients, K_{pj} and K_{dj} are the coordination term coefficients; $y_{ij}(t_{k+1})$ and $\dot{y}_{ij}(t_{k+1})$ are the displacement measurement information and velocity measurement information at time t_{k+1}.

The dynamic model of the LSTS is given by the proposed MDMA. The material parameters of the substructure are shown in Table 1. There are three types of substructure controllers, including the one with information coordination term on the right side; the one with information coordination terms on both sides, and the one with information coordination term on the left side. The parameters of the distributed cooperative controller in the assembly process are displayed in

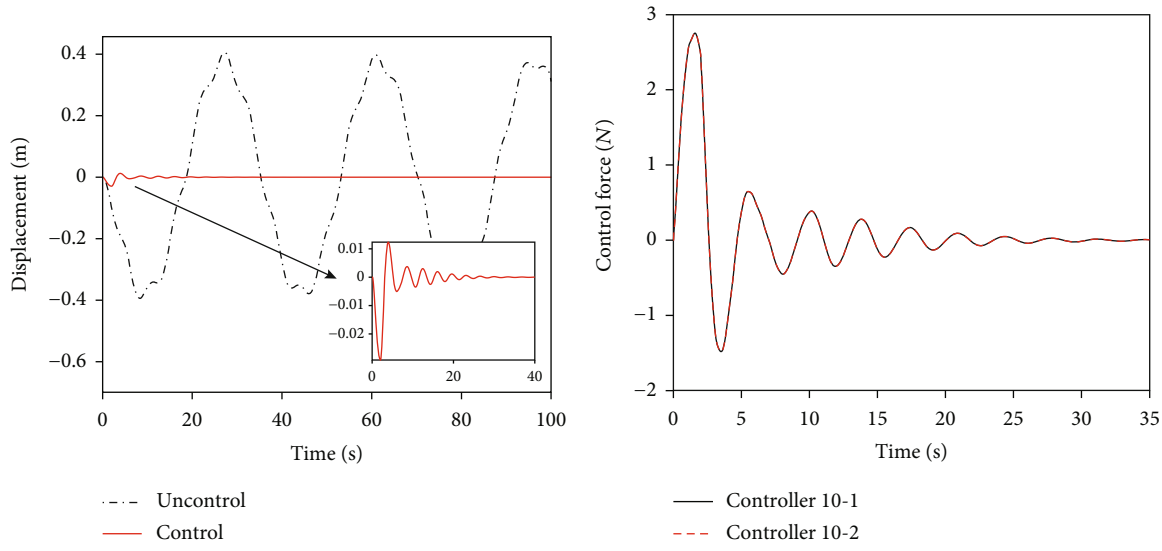

(a) The end dynamic response of truss structure

(b) The control force of the 10th substructure

FIGURE 11: The dynamic response and the control force during the 10th assembly stage.

$$\begin{aligned} U_1 &= 100y_1 + 5\dot{y}_1 + 10(y_1 - y_2) + (\dot{y}_1 - \dot{y}_2), \\ &\cdots \\ U_i &= 100y_i + 5\dot{y}_i + 10(y_{i-1} - y_i) + (\dot{y}_{i-1} - \dot{y}_i) + 10(y_{i+1} - y_i) + (\dot{y}_{i+1} - \dot{y}_i), \\ &\cdots \\ U_n &= 100y_n + 50\dot{y}_n + 10(y_{n-1} - y_n) + (\dot{y}_{n-1} - \dot{y}_n). \end{aligned} \tag{24}$$

The impact disturbance force is simulated by the step excitation.

$$W = \begin{cases} 2N, & 0 \le t \le 2s \\ 0N, & 2s \le t \le t_{\text{end}} \end{cases}. \tag{25}$$

The total length of the LSTS is 97.5 m and 195 m after the 5th and the 10th group truss substructure is assembled, respectively. The z-axis displacement at the end nodes of the LSTS is obtained, as shown in Figures 10 and 11. The distributed cooperative controller (Eq. (23)) is used to suppress the vibration during on-orbit assembly. The vibration amplitude is significantly suppressed compared to the vibration response before control, which is suppressed within 15 s and 30 s. The control force of the end substructure is kept within 3 N. The number of controllers increases gradually with the progress of the on-orbit assembly, and the vibration can be quickly suppressed, which indicates that the proposed controller has good expansibility. Moreover, it is also noted that the proposed dynamics model is suitable for active vibration suppression during on-orbit assembly of LSTS.

5. Conclusion

The dynamic modeling problem of large-scale space structures during on-orbit assembly process is investigated. The modeling process and constraint conditions are first presented. The MDMA is then proposed, which can be used for the dynamic modeling of a LSS in the assembly process. Finally, the LSTS is chosen as the research object, and the numerical examples are provided, including a distributed cooperative controller. The results demonstrate that (1) the coefficient matrices of the adjacent substructure are decoupled, and the reconfiguration of the existing coefficient matrices is not required along with the assembly using the proposed MDMA. The extra calculation due to the coupling of state coefficient matrices of the LSS at each assembly stage is avoided. (2) The proposed dynamic model can accurately describe the dynamic characteristics of the incrementally increasing space structure. (3) The vibration of the LSS is well suppressed during on-orbit assembly. The controller is designed based on the MDMA, which has good control performance and expansibility.

Data Availability

The data used to support the findings of this study are available from the corresponding author upon request.

Conflicts of Interest

The authors declare that they have no known competing financial interests or personal relationships that could have appeared to influence the work reported in this paper.

Acknowledgments

This work is supported by the National Natural Science Foundation of China (grant numbers 11972102, 12232015, and 62203033) and the Fundamental Research Funds for the Central Universities, Sun Yat-sen University (No. 22qntd0703).

References

[1] C. F. Lillie, "On-orbit assembly and servicing of future space observatories," in *Space Telescopes and Instrumentation I: Optical, Infrared, and Millimeter*, pp. 767–778, Orlando, FL, USA, 2006.

[2] L. Datashvili, S. Endler, B. Wei et al., "Study of mechanical architectures of large deployable space antenna apertures: from design to tests," *CEAS Space Journal*, vol. 5, no. 3-4, pp. 169–184, 2013.

[3] C. Yang, W. Lu, and Y. Xia, "Uncertain optimal attitude control for space power satellite based on interval Riccati equation with non-probabilistic time-dependent reliability," *Aerospace Science and Technology*, vol. 139, 2023.

[4] W. Li, D. Cheng, X. Liu et al., "On-orbit service (OOS) of spacecraft: a review of engineering developments," *Progress in Aerospace Sciences*, vol. 108, pp. 32–120, 2019.

[5] P. Boning and S. Dubowsky, "Coordinated control of space robot teams for the on-orbit construction of large flexible space structures," *Advanced Robotics*, vol. 24, no. 3, pp. 303–323, 2010.

[6] S. S.-M. Swei, B. Jenett, N. B. Cramer, and K. Cheung, "Modeling and control of robot-structure coupling during in-space structure assembly," in *AIAA Scitech 2020 Forum*, p. 1544, Orlando, FL, USA, 2020.

[7] J. Katz, S. Mohan, and D. Miller, "On-orbit assembly of flexible space structures with SWARM," in *AIAA Infotech@ Aerospace 2010*, p. 3524, Atlanta, GA, USA, 2010.

[8] C. Liu, X. Yue, J. Zhang, and K. Shi, "Active disturbance rejection control for delayed electromagnetic docking of spacecraft in elliptical orbits," *IEEE Transactions on Aerospace and Electronic Systems*, vol. 58, no. 3, pp. 2257–2268, 2021.

[9] B. Lyu, C. Liu, and X. Yue, "Hybrid nonfragile intermediate observer-based T-S fuzzy attitude control for flexible spacecraft with input saturation," *Aerospace Science and Technology*, vol. 128, 2022.

[10] K. Zhang, S. Wu, and Z. Wu, "Multibody dynamics and robust attitude control of a MW-level solar power satellite," *Aerospace Science and Technology*, vol. 111, 2021.

[11] B. Duan, "The main aspects of the theory and key technologies about space solar power satellite," *Scientia Sinica Technologica*, vol. 48, no. 11, pp. 1207–1218, 2018.

[12] J. Ding, F. Gao, X. Zhong et al., "The key mechanical problems of on-orbit construction," *Scientia Sinica Physica, Mechanica & Astronomica*, vol. 49, no. 2, 2019.

[13] E. Wang, S. Wu, and Z. Wu, "Active-control-oriented dynamic modelling for on-orbit assembly space structure," *Chinese Journal of Theoretical and Applied Mechanics*, vol. 52, no. 3, pp. 805–816, 2020.

[14] D. Wang, X. Shao, and S. Liu, "Assembly sequence planning for reflector panels based on genetic algorithm and ant colony optimization," *The International Journal of Advanced Manufacturing Technology*, vol. 91, no. 1-4, pp. 987–997, 2017.

[15] K. Cao, S. Li, Y. She, J. D. Biggs, Y. Liu, and L. Bian, "Dynamics and on-orbit assembly strategies for an orb-shaped solar array," *Acta Astronautica*, vol. 178, pp. 881–893, 2021.

[16] S. Wu and W. Zhou, "Vibration control for large space truss structure assembly using a distributed adaptive neural network approach," *Acta Astronautica*, vol. 212, pp. 29–40, 2023.

[17] E. Wang, S. Wu, G. Xun, Y. Liu, and Z. Wu, "Active vibration suppression for large space structure assembly: a distributed adaptive model predictive control approach," *Journal of Vibration and Control*, vol. 27, no. 3-4, pp. 365–377, 2021.

[18] C. Yang and Q. Yu, "Placement and size-oriented heat dissipation optimization for antenna module in space solar power satellite based on interval dimension-wise method," *Aerospace Science and Technology*, vol. 134, 2023.

[19] J. Chung and G. Hulbert, "A time integration algorithm for structural dynamics with improved numerical dissipation: the generalized-α method," *Journal of Applied Mechanics the ASME*, vol. 60, no. 2, pp. 371–375, 1993.

[20] W. Zhou, K. Zhang, S. Wu, S. Tan, and Z. Wu, "Distributed cooperative control for vibration suppression of a flexible satellite," *Aerospace Science and Technology*, vol. 128, 2022.